



ELSEVIER

Contents lists available at ScienceDirect

Corrosion Science

journal homepage: www.elsevier.com/locate/corsci

Investigation of the passive layer on a solid-state sintered silicon carbide ceramic formed in sulfuric acid

M. Schneider^{a,*}, K. Kremmer^a, M. Voigt^b, G. Grundmeier^b

^a Fraunhofer IKTS Dresden, Winterbergstr. 28, 01277, Dresden, Germany

^b Paderborn University, Technical and Macromolecular Chemistry, Warburgerstr. 100, 33098, Paderborn, Germany

ARTICLE INFO

Keywords:

Solid-state sintered silicon carbide

Passivity

EIS

XPS

ABSTRACT

The presented work considers the electrochemical oxidation of solid-state sintered silicon carbide as a widely used structural material. The passive behavior, oxide formation and the structure of the near-surface region are characterized by means of cyclic voltammetry, electrochemical impedance spectroscopy, and XPS studies. Electrochemical measurements and complementary surface analytical studies reveal the formation of a near-surface region which can be described as amorphous non-stoichiometric SiO_x , SiO_xC_y . After polarization at 1500 mV_{SCE} the thickness of this oxidized region is in the range of 4–5 nanometers. The formation reaction of SiC to SiO_x is explained by a 4-electron mechanism under the formation of carbon. Additionally, anodic oxygen evolution must be assumed to 20 %–30 % efficiency at this potential.

1. Introduction

SiC is a wide-bandgap semiconductor with manifold applications in (micro-) electronic applications and various microsystems [1–3]. In this context, the (photo-)electrochemical properties of SiC themselves were previously investigated in the 1970s (see inter alia [4–6]). Characterizing the photoelectrochemical generation of hydrogen of aluminum doped SiC single crystals, Bockris et al. [6] determined the flatband potential of SiC to 1.68 V_{SHE} in 0.5 M H₂SO₄. Later, Lauermann et al. extended the investigation on various polytypes of SiC [7]. Due to the bandgap and the chemical stability, the authors assumed that electrochemical corrosion of SiC is not relevant under the specific conditions of the photoelectrolysis of water [7]. Schnabel et al. have shown that the pH-value of the electrolyte greatly influenced the flatband potential of p-doped α -SiC [8]. Mathews et al. [9] showed similar tendencies but different absolute values (flatband potential -0.2 V_{SCE} at pH 1). A comparison of the literature demonstrates the expectable high impact of the exact composition and doping level of SiC as well as the electrolyte on the material properties. Currently, SiC-based nanostructured and porous materials are widely discussed as super-capacitors [10–14]. However, these papers are focused on the study of non-faradaic processes and do not address corrosion relevant electrochemical behaviors.

Less studied but of high relevance, SiC is also the basis of high-performance ceramics applied as structural material [15,16]. A

representative silicon carbide based ceramic are so-called solid-state sintered silicon carbide ceramics (SSiC). This material is widely used for seals, slide bearings or valves in industry under varying corrosive environments [15]. SSiC-ceramics rank as a material with outstanding chemical and corrosion stability in many media and different conditions including a good stability in hydrofluoric acid [7,15,17–19]. However, SSiC shows a very wide range of resistivity from 10⁶ Ωm to 1 Ωm depending on the process technology and the sinter additives used (e.g. B, Al). These sinter additives are commonly completely incorporated into the SiC grains, act as dopant and enhance the conductivity of the SSiC-ceramic [20]. Meschke et al. [21] published damage patterns of SSiC seals which suggest electrochemical corrosion as matter. Furthermore, they declare the formation of SiO₂ on SSiC in cold water. Divakar et al. [22] applied various common electrochemical corrosion tests at first to investigate the corrosion rate of SiC-ceramics in inorganic acids. They assumed the dissolution of Si to Si⁴⁺ and reported a corrosion current density of approximately 0.01 $\mu\text{A cm}^{-2}$ for sintered α -SiC in 70 % HNO₃ calculated according the Stern-Geary relationship. Cook et al. [23] used the same procedure and calculated approximately 7 $\mu\text{A cm}^{-2}$ for SSiC in 1 M H₂SO₄. Based on the Pourbaix diagram they assumed the oxidation of SiC to SiO₂, which passivates the surface. Andrews et al. [24] postulated the formation of SiO₂-passive film on SSiC in nitric acid and determined a corrosion current density to 58 $\mu\text{A cm}^{-2}$. Summarizing the literature the following anodic half reactions on SiC-ceramics are discussed (see e.g. [25,26,27,28,29]):

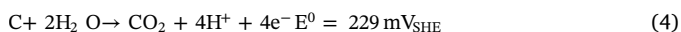
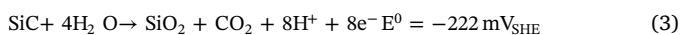
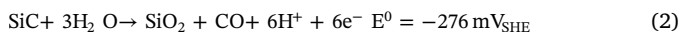
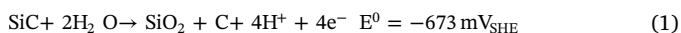
* Corresponding author.

E-mail address: michael.schneider@ikts.fraunhofer.de (M. Schneider).

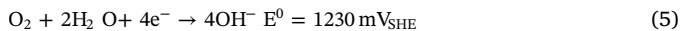
<https://doi.org/10.1016/j.corsci.2020.108690>

Received 26 September 2019; Received in revised form 9 April 2020; Accepted 16 April 2020

0010-938X/ © 2020 Elsevier Ltd. All rights reserved.



Depending on the potential, the oxygen reduction or the hydrogen reduction can be assumed as cathodic half reactions:



According to the Eqs. 1–3, it can be assumed that the corrosion behavior of SSiC-ceramics in acidic solution is determined by the formation of a SiO_2 passive layer. Andrews et al. [24,29] assume the passive film formation according to Eq.1 and found a thin carbon layer on the surface after corrosion in an acidic electrolyte. Again, all other authors favor the formation of silicon oxide according Eqs.2 or 3. However, the composition of this passive layer on technical SSiC is so far hardly investigated in detail. In contrast to the aforementioned assumption, Lavrenko et al. [30] assume the formation of metastable H_2SiO_3 followed by a dissociation to HSiO_3^- in sulfuric acid at open circuit potentials. This is in contradiction to Sydow et al. who calculated a Pourbaix diagram SiC-water based on thermodynamically available data and show that HSiO_3^- is thermodynamically instable under acidic conditions [25]. After anodic polarization in the passive range, Lavrenko et al. reported the formation of an oxycarbide $\text{SiC}_{0.67}\text{O}_{0.33}$ layer. Indeed, oxycarbides are also mentioned as tribochemical reaction products [31].

In the work presented here the authors focus on the corrosion behavior of a commercially available SSiC material in sulfuric acid and the development of the passive film properties at advancing anodic polarization potential. Surface analysis (XPS, SEM) supplements the study of the passive film formation and evidence the complexity of the passivity of technical SSiC-ceramics.

2. Materials and methods

2.1. Material

The material used was a solid-state sintered silicon carbide ceramic (SSiC) with the tradename EKasic® D (ESK Ceramics GmbH). The material consists of α -SiC containing a small amount of aluminum (0.3 wt %) [32]. As aforementioned, aluminum acts as a doping element and increases the electric conductivity ($\sigma = 0.01 \dots 0.1 \text{ S cm}^{-1}$) [32,33]. Process-related, the SSiC contains a small amount of carbon precipitates (in this case approximately 1.6 % of the surface area) and a small number of tiny pores.

All samples were mechanically pretreated, subsequently polished with a diamond suspension up to 1 μm diamond grain sizes and rinsed with deionized water. The samples were dipped in a diluted hydrofluoric acid (1 wt%) for 5 min prior to the electrochemical experiments to remove preexistent surface films and again rinsed with deionized water.

2.2. Methods

2.2.1. Electrochemistry

Electrochemical experiments were carried out in a flat cell using a 3-electrode design. A saturated calomel electrode (Sensortechnik Meinsberg) worked as reference and a platinized titanium expanded metal as counter electrode. All electrochemical measurements were performed by an electrochemical workstation Autolab 30 (Metrohm) including potentiostat, scan generator and frequency analyzer coupled with a personal computer.

The electrolyte used was 0.5 M sulfuric acid (pH 0.3, $\sigma = 0.2$

Scm^{-1}) at ambient temperature.

The EIS-study was carried out as staircase experiment. Before the impedance measurement started, the sample was polarized over 10 min at the respective potential. The polarization potential was stepwise increased immediately after executing the impedance spectroscopy.

2.2.2. X-ray photoelectron spectroscopy (XPS)

XPS analytical studies were performed by means of an Omicron system with a monochromatic Al X-ray source. The spot size was approximately 800 microns. The chamber base pressure was below 3×10^{-10} mbar. The survey spectra were measured in a range from 0 to 1200 eV with a dwell time of 200 ms, a pass energy of 100 eV and steps of 0.5 eV. For the elemental spectra the pass energy was set to 20 eV with steps of 0.1 eV. CasaXPS version (2.3.15) software package was used for peak deconvolution and compositional analysis. All spectra were measured at an angle of 60° .

A Lorentz–Gauss cross-product function in combination with Shirley background was utilized as common line-shape. For the conductive graphitic compound an asymmetric C 1s peak-shape (A(0.25,0.38,20) GL(20)) was employed for deconvolution. The CasaXPS database of relative sensitivity factors (RSF) was used for quantification of atomic concentrations.

Sputter profiling was performed using a “FIG-5” ion gun from Ulvac-Phi and argon as sputter gas. The source to normal angle was 30 degree; take-off angle for these XPS measurements was 30 degree. After removing adventitious carbon at energy of 300 eV for 30 s the energy for sputtering was changed to 2000 eV.

3. Results and discussion

3.1. Electrochemical measurements

Fig.1 shows the open circuit potential (ocp) of EKasic® D in sulfuric acid immediately after pre-treatment in hydrofluoric acid. Initially the potential rises from $E = -170 \text{ mV}_{\text{SCE}}$ to $-80 \text{ mV}_{\text{SCE}}$ over the first 60 min. and reaches a plateau at about $E = -100 \text{ mV}_{\text{SCE}}$ after 90 min. The observed development of the ocp can be explained by a passive film formation on the freshly prepared samples. The value of the ocp suggests a mixed potential between the oxidation of SiC (Eq. 4) and cathodic oxygen reduction (Eq. 5). Both reactions are kinetically limited by the formation of a very thin SiO_x film.

Fig. 2a shows two scans of a cyclic voltammogram on EKasic® D starting at $E = -800 \text{ mV}_{\text{SCE}}$. The anodic sweep of the 1st scan shows hydrogen evolution up to a potential of $-500 \text{ mV}_{\text{SCE}}$, a current peak with a maximum at $230 \text{ mV}_{\text{SCE}}$ suggesting at a first glance the active dissolution and passivation of SiC and finally a transpassive region

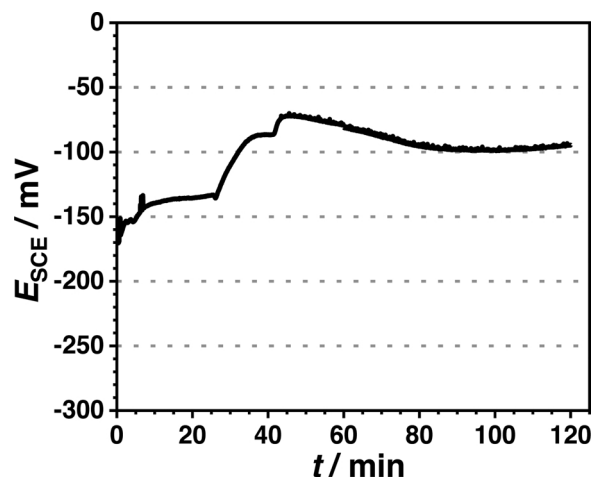


Fig. 1. Open circuit potential of EKasic®D measured in 0.5 M H_2SO_4 electrolyte.

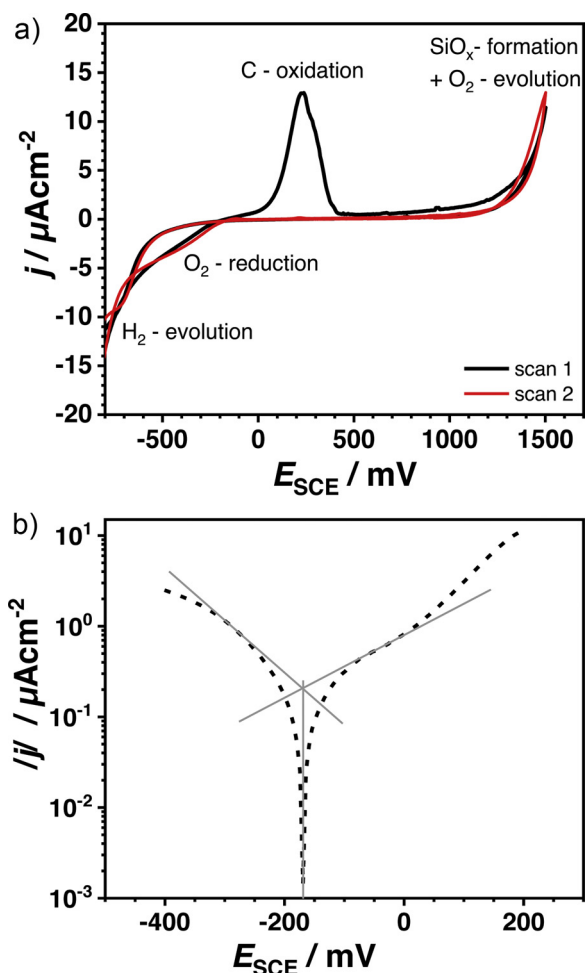


Fig. 2. a) Cyclic voltammetry on EKasic®D in 0.5 M H₂SO₄ (dE/dt = 1 mVs⁻¹). b) Semi-logarithmic plot of a section of the 1st anodic sweep shown in Fig.2a.

associated with anodic oxygen evolution.

The consumed charge covered by the oxidation peak at 230 mV_{SCE} integrates to $q \approx 3 \text{ mC cm}^{-2}$. If this charge was exclusively caused by a passivation of SiC and assuming 100 % efficiency of the oxide formation the passive film growth (Δd_{ox}) would be calculated to a thickness of 1 nm ($z = 8$), 1.5 nm ($z = 6$) and 2 nm ($z = 4$), respectively.

$$\Delta d_{ox} = \frac{qM}{zF\rho} \quad (7)$$

M is the molar mass of SiO₂ (60 g cm⁻³), F represents the Faraday constant, ρ the density of amorphous SiO₂ (2.2 g cm⁻³ [34]) and z the number of consumed electrons.

So far, native oxide thickness values on SSiC are not yet published but Carim et al. [35] reported a native oxide thickness of $d_0 = 0.5\text{--}1.5 \text{ nm}$ on silicon wafers shortly after etching in HF. Consequently, the overall passive film thickness $d = d_0 + \Delta d_{ox}$ formed at potentials more positive than 230 mV_{SCE} should be about 1.5 and 3.5 nm respectively. However, this expectation could not be confirmed by the measured XPS data (see discussion below). Additionally, the manifestation of the peak at 230 mV_{SCE} seems to depend on randomly variation of the pretreatment and the intensity is less reproducible. In previous measurements, for example, the peak at 230 mV_{SCE} was not observed which might be due to the different pre-treatment procedures [20]. In contrast to the previous study, the sample analyzed in the presented study was mechanically polished and thereafter shortly etched in hydrofluoric acid to remove the native oxide layer prior to the electrochemical experiment. Thereby, the authors assume that this pre-

treatment resulted in a thin film of carbon on the surface which originates from minor carbon precipitation. The latter is known to remain in the material due to the sintering process. Finally, the peak at 230 mV_{SCE} seems to represent the oxidation of this thin carbon film according to Eq. 4. After the oxidation, the carbon film is removed and does not appear in the second scan.

At approximately 1300 mV_{SCE} the current rises again. Visual post-experiment examinations did not reveal any corrosive attack and consequently the authors explain the current rise by both anodic formation of SiO_x (Eqs. 1–3) associated with anodic oxygen evolution (Eq. 5). According to Bockris et al. the anodic oxygen evolution requires the existence of a thin oxide film and vice versa. The anodic oxygen evolution indicates the existence of an oxide film on the surface [36]. The anodic evolution of oxygen on SiC is controversially discussed in the literature. Lauerman et al. [7] negate the existence of anodic oxygen evolution below 2V_{SCE} and assumed corrosion. Others report of anodic evolution of oxygen on α -SiC at similar potentials in sulfuric acid [30,37].

During the return sweep the current drops down to almost zero. No re-activation of the sample is observed. The increasing negative current density below $E \approx -150 \text{ mV}_{SCE}$ is caused by oxygen reduction first (Eq. 5) followed by strong hydrogen evolution (Eq.6).

A consideration of the 1st anodic sweep shown in Fig. 2a close to the corrosion potential is separately plotted in Fig. 2b. The corrosion potential ($E_{corr} = -170 \text{ mV}_{SCE}$) fits very well with the open circuit potential discussed in Fig. 1. The corrosion current density is calculated to $j_{corr} = 0.2 \mu\text{A cm}^{-2}$. The graphic estimation of the Tafel-lines results to Tafel-coefficients $b_a = 290 \text{ mV dec}^{-1}$ and $b_c = 170 \text{ mV dec}^{-1}$ respectively. Such Tafel-coefficients indicate a restrained charge transfer due to the influence of the native passive film on the surface.

Nevertheless, the nature of the surface of the SSiC ceramic EKasic® D under acidic conditions can not be completely understood based on CV measurements alone. Therefore, the passive behavior of the material was additionally investigated by means of electrochemical impedance spectroscopy. Before the EIS measurement, the sample was potentiostatically polarized over 10 min at different potentials and the current density was recorded. The steady state current density (passive current density) during the polarization and EIS measurement, respectively, was quite low and led to current densities below $j \leq 0.5 \mu\text{A cm}^{-2}$. Except at potentials of 1500 mV_{SCE} the stationary current density was increased up to $50 \mu\text{A cm}^{-2}$. Fig. 3 represents the collection of all impedance spectra as Bode-plots.

The measured spectra apparently show only one time constant ($\tau = R \cdot C$). Therefore, the equivalent circuit shown in Fig. 4 is used for the fitting routine and calculating the values of the equivalent elements as shown in Table 1.

The high frequency range is dominated by an ohmic resistance. However, this resistance is calculated to $R_{\Omega} = 83 \Omega\text{cm}^2$ (Table 1). Regarding the electrolyte resistivity ($\rho = 4.5 \Omega\text{cm}$) this resistance cannot be solely explained by the electrolyte resistance. Instead, regarding the sample geometry, R_{Ω} is mainly determined by the resistivity ρ of the ceramic sample it-self. A calculation of the resistivity reveals $\rho \approx 80 \Omega\text{cm}$ that well agrees with manufacturer's data [32]. Similar to an electrolyte resistance, R_{Ω} does not change depending on the applied potential or time of experiment respectively.

The capacitance C calculated from the capacitive reactance X_c in the mid-frequency range is likewise constant over all experiments and independent of the prior polarisation. Assuming that the capacitance represents the dielectric properties of an SiO₂-like layer ($\epsilon_r \approx 4.5$ [38]) or SiOC-layer ($\epsilon_r \approx 3$ [39]), the calculated passive film thickness is in the range of $d_{ox} \approx 0.25\text{--}0.4 \text{ nm}$. Such a film thickness would correspond to a mono- or bilayer of silica [40] and fits to the reported thickness of native oxide films on silicon, which ranges between 0.2 and 1.5 nm depending on the doping level [35,41,42]. Indeed, as the authors discuss later on in Section 3.2, the XPS-data of the sample "Reference" (untreated, covered by a native oxidized surface) as well as the samples

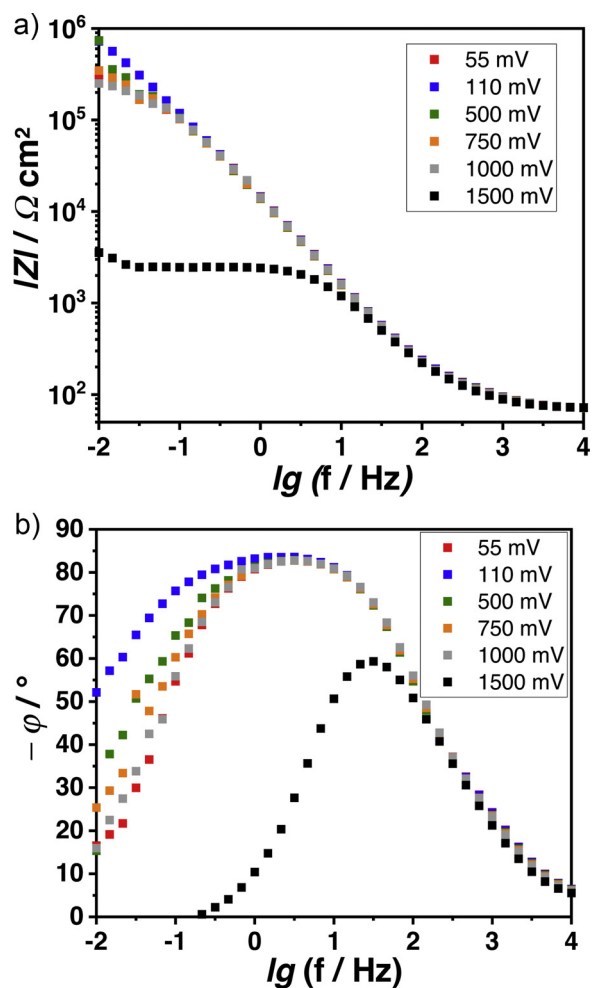


Fig. 3. a) Bode-plot (magnitude) of the impedance spectra measured on EKasic®D in 0.5 M H_2SO_4 . b) Bode-plot (phase shift) of the impedance spectra measured on EKasic®D in 0.5 M H_2SO_4 .

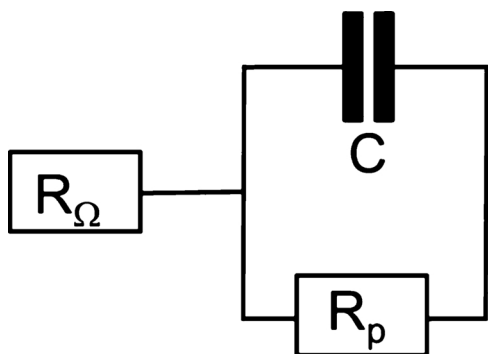


Fig. 4. Equivalent circuit representing the resistance of the sample and the electrolyte (R_Ω), the passive film capacitance (C) and the polarization resistance (R_p).

“P55” and “P750” representing the samples after polarization at 55 mV_{SCE} and 750 mV_{SCE} , respectively, show no evidence of anodically formed SiO_x . Nevertheless, the slight asymmetry of the Si 2p peak suggests the existence of a very thin surface film, which can be described as non-stoichiometric SiO_xC_y . The latter composition is characteristic for the native passive film on SiC. The thickness of this film is more or less stable and the measured capacitance is unaltered. In other words the measured capacitance is actually caused by the very thin native oxide film and reflects the dielectric properties of this film. After

Table 1

Values of resistance and reactance of the spectra (Fig. 3) calculated by fitting the spectra on the measured data by using the equivalent circuit shown in Fig. 4.

$E_{\text{pot}} / \text{mV}_{\text{SCE}}$	$R_\Omega / \Omega \text{ cm}^2$	$C / \mu\text{Fcm}^{-2}$	$R_p / \text{k}\Omega \text{ cm}^2$	τ / s
55	83	10	213	2.1
110	83	11	824	9.1
500	82	12	323	3.8
750	83	11	249	2.8
1000	82	11	212	2.3
1500	82	10	2	0.02

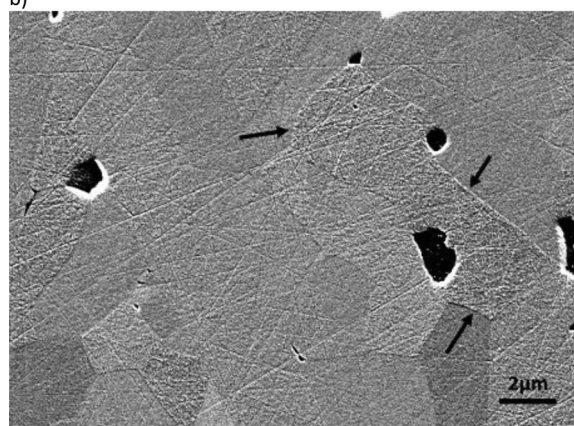
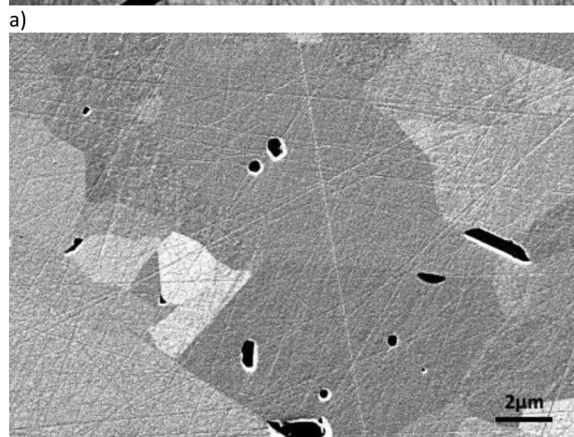
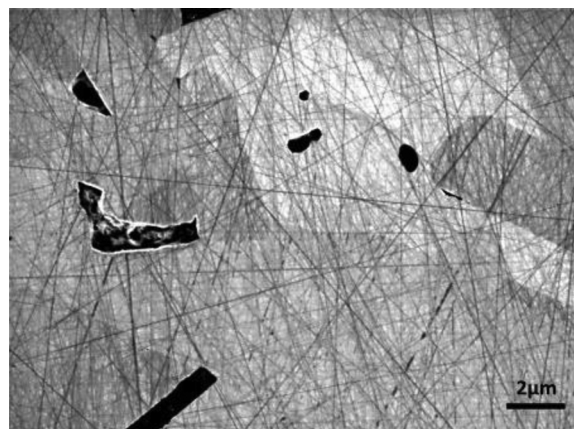


Fig. 5. SEM image of the sample before the electrochemical experiment (a); after potentiostatic polarization at $E = 750 \text{ mV}_{\text{SCE}}$ (b) and at $E = 1500 \text{ mV}_{\text{SCE}}$ (c).

Table 2
XPS analysis of the surface composition of the studied samples.

Survey	Transition	Position (eV)	FWHM (eV)	%-at	C:Si	O:(Si + C)
Reference	O 1 s	531	3.0	11.1	2.3:1	0.12:1
	C 1 s	284	3.2	61.0		
	N 1 s	398.5	3.3	0.7		
	Si 2p	99	3.0	27.0		
	Al 2p	71	3.0	0.2		
Sample P55 ($E_{dc} = 0.55$ V (SCE))	O 1 s	531.5	3.1	12.7	1.5:1	0.15:1
	C 1 s	283.5	5.2	51.4		
	N 1 s	399.5	3.1	1.6		
	Si 2p	99.5	2.8	34.1		
	Al 2p	71.5	2.4	0.3		
Sample P750 ($E_{dc} = 0.75$ V (SCE))	O 1 s	532.5	2.7	12	1:1	0.12:1
	C 1 s	283	3.3	43.3		
	N 1 s	400.5	3.7	1.0		
	Si 2p	100	2.6	43.1		
	Al 2p	73.0	2.6	0.4		
Sample P1500 ($E_{dc} = 1.5$ V(SCE))	O 1 s	532.5	2.8	31.1	2.1:1	0.46:1
	C 1 s	284.5	3.1	45.6		
	N 1 s	400	3.1	1.6		
	Si 2p	103	3.3	21.7		
	Al 2p	1486.7	–	–		

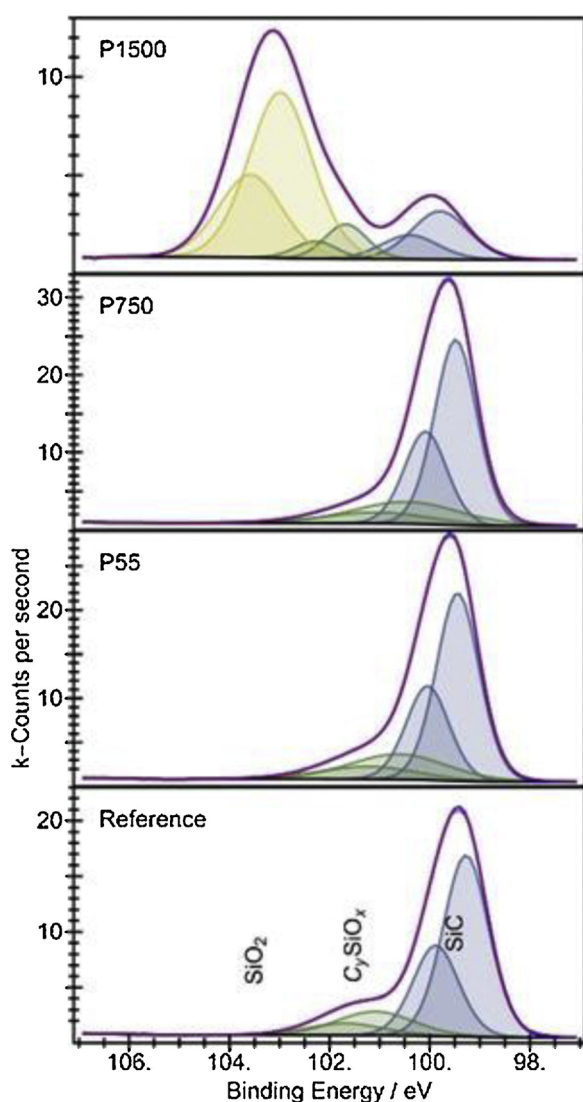


Fig. 6. Element spectra of silicon (Si2p) in the near-surface region measured at a take-off angle of 60°.

the polarization at 1500 mV_{SCE} (“P1500”) the spectrum is significantly changed. The resistance at low frequency range drops down to 2 kΩ cm² but the capacitance is still approximately 10 μF cm⁻². However, the XPS-data clearly show the existence of anodically formed SiO_x and allow for the estimation of an oxide thickness of 4–5 nm. To validate this value, the authors complementarily calculated the oxide film thickness using Eq. 7 after the polarization at 1500 mV_{SCE} over 10 min (pre-polarization time before EIS). Assuming the formation of silicon oxide via the 4-electron reaction according Eq. 1 and 70 % current efficiency due to the simultaneously proceed oxygen evolution the thickness of the oxide film was calculated to 5 nm, which fits very good the XPS-data. Based on this thickness, the calculated effective relative permittivity amounts to $\epsilon_r \approx 50$. This high value can only be explained by a significant incorporation of water and hydrated ions in the nanoporous amorphous surface layer [43]. The incorporation of a significant amount of water is well known for anodically formed silicon oxide [44]. Such a nanoporous layer also explains the on-set of oxygen evolution measured by cyclic voltammetry. The thin nanoporous layer obviously allows the electron transfer due to the resonance tunneling process [45,46].

Consequently, the surface layer does not act as a perfect dielectric barrier but can be rather described as a three dimensionally crosslinked few nanometer thin nanoporous and defect-rich film.

The ohmic resistance, which dominates the spectra in the low frequency range, can be interpreted as polarization resistance R_p , which is almost the resistance of the passive layer formed on the SiC grains. The value is in the range of $10^5 - 10^3 \Omega \text{ cm}^2$, which is similar to the passive behavior of FeCr25 alloys in sulfuric acid [47]. Considering the oxide film thickness of few nanometers, the calculated resistivity is in the range of $10^9 \Omega \text{ cm}$ to $10^{12} \Omega \text{ cm}$. For comparison, the resistivity of anodic formed oxide on crystalline silicon carbides is reported between $10^{12} \Omega \text{ cm}$ to $10^{16} \Omega \text{ cm}$ [48]. The relatively low values support the aforementioned discussion of the nature of passive films considering water incorporation and formation of silica. The aforementioned presence of water exponentially influences the resistivity of silica gel as reported by Anderson et al. [49].

The SEM images (Fig. 5a–c) indicate that the substrate does not experience any measurable dissolution process during polarization at $E = 750$ mV_{SCE} as well as $E = 1500$ mV_{SCE}. After polarization at $E = 1500$ mV_{SCE} (see Fig.5c), the SEM analysis indicates the existence of the anodic oxidized surface and different thickness for different grains (see the black arrows in Fig. 5c). These results are in good agreement with the former study reported by Herrmann et al. [20].

Table 3
Analysis of the XPS C1 s element spectra of the studied samples.

C1 s	Peak assignment	Position (eV)	FWHM (eV)	at-%	References
Reference	SiC	281.9	1.2	26.2	281.3–283.5 eV [55]
	Carbon	284.5	1.2	69.0	centred at 284.5 eV
	C–O	286.2	1.2	3.1	286.3–286.7 eV [55]
	C=O,COOH	288.7	1.2	1.8	287.8–289.5 eV [55]
P55	SiC	282.2	1.2	39.8	282.7–283.2 eV [54]
	Carbon	284.5	1.4	50.8	centred at 284.5 eV
	C–O	286.3	1.1	5.8	[54]
	C=O,COOH	288.1	2.0	3.7	[54]
P750	SiC	281.7	1.0	67.2	282.7–283.2 eV [54]
	Carbon	284.2	1.6	24.9	centred at 284.5 eV
	C–O	285.8	1.1	5.3	[54]
	C=O,COOH	287	2.0	2.6	[54]
P1500	SiC	282.0	1.4	5.7	282.7–283.2 eV [54]
	Carbon	284.5	1.3	77.6	centred at 284.5 eV
	C–O	286.2	1.3	10.8	[54]
	C=O,COOH	288.2	1.8	5.9	[54]

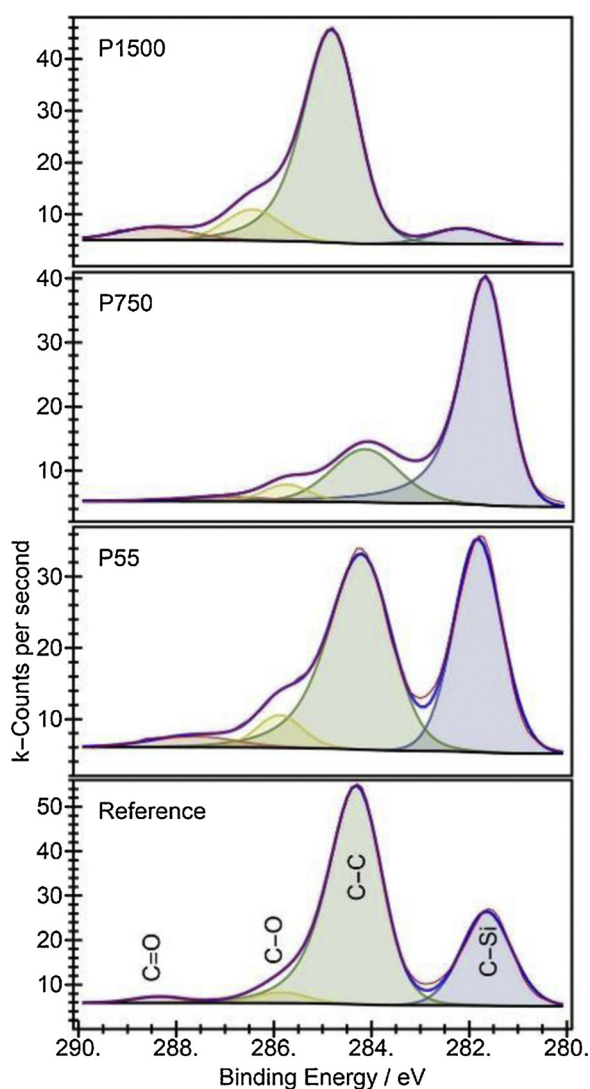


Fig. 7. Element spectra of carbon (C1 s) in the near-surface region measured at a take-off angle of 60°.

They found different passive layer thickness values after polarization depending on the polytype of SiC grains, but not on their crystallographic orientation.

3.2. X-ray photoelectron spectroscopy (XPS)

The near-surface region of the electrochemically oxidized surfaces was analyzed by means of XPS. The data of the survey spectra are shown in Table 2. For sample “P1500” (representing the sample after polarization at $E = 1500 \text{ mV}_{\text{SCE}}$), the electrochemical oxidation led to a strong increase of the surface concentration of oxygen while the corresponding oxygen concentration, for sample “P55” is only slightly higher than for the reference state. Obviously, the ratio C:Si is in the range between 1 and 2.3 : 1 for all studied samples. The ratio C:Si of about 1:1 for sample “P750” indicates a strongly reduced amount of surface carbon by the electrochemical oxidation process.

The Si2p element spectra shown in Fig. 6 and listed in Table 3 suggest that the near-surface regions of the reference sample and sample “P55” mainly consist of SiC. However, the surfaces of sample „P55” and the reference are partially oxidized as part of the silicon atoms are observed in oxidation states which are characteristic for silicon coordinated to about two oxygen atoms [50]. For sample “P55” and “P750”, no SiO_x was observed in the near-surface region. However, the element spectra in Fig. 6 show that the near-surface region of the sample P1500 clearly consists of SiO_x . Based on the at-% ratio of SiO_x/SiC and the given take-off angle during the measurement one can assume that the thickness of the surface SiO_x film for sample “P1500” was about 4–5 nm. This estimation is based on the hypothesis that a continuous thin SiO_2 -film is formed. The equation

$$\frac{I_m}{I_o} = \frac{N_m \lambda_m \exp[-(d/\lambda_o \sin\theta)]}{N_o \lambda_o (1 - \exp[-(d/\lambda_o \sin\theta)])} \quad (8)$$

were I , d , N , θ and λ represents the intensity, the layer thickness (nm), the volume densities of Si atoms, the electron take off angle and inelastic mean free path (m : SiC and o : SiO_2) used for layer thickness calculation, is used to calculate the surface film thickness [51,52].

The C1 s high resolution data are presented in Fig. 7 and listed in Table 4. Already the reference sample shows small contributions of C–O and C=O in addition to the dominating C–Si and C–C/C–H contributions. Due to the ex-situ analytical approach adventitious could contribute this signal. The C–C and C–H contribution at 284.2 eV could originate from the preparation process of the sample. However, the concentration of oxidized carbon species is significantly increased for sample “P55” indicating a clearly higher oxidation state than for the reference sample. Moreover, the C–C/C–Si ratio is decreased in comparison with the reference state. “P750” shows the lowest C–C rate. One could argue that the surface carbon layer of the reference sample is

Table 4
Analysis of the Si2p element spectra of the studied samples.

Si 2p	Peak assignment	Position (eV)	FWHM (eV)	at-%	Reference
Reference	SiC	99.3	1.1	41.3	100.4 eV–101 eV [55]
		99.9	1.1	40.5	
	SiO _x C _y	101.1	1.8	9.2	for x = 0–1.93
P55	SiC	101.7	1.8	9.0	99.8 eV–103.1 eV [50]
		99.4	1.0	38.7	
	SiO _x C _y	100.0	1.0	38.0	100.4 – 100.7 eV [54]
		100.6	2.3	11.8	
P750	SiC	101.2	2.3	11.6	99.1 eV–101.1 eV [53]
		99.5	1.0	38.9	
	SiO _x C _y	100.1	1.0	38.1	
		100.5	2.5	11.6	
P1500	SiC	101.1	2.5	11.4	
		99.8	1.3	9.4	
	SiO _x C _y	100.4	1.3	9.2	100.4 – 100.7 eV [54]
		101.7	1.0	5.0	
		102.3	1.0	4.9	
SiO ₂	103.0	1.5	36.1	103.2 eV – 104 eV [55]	
	103.6	1.5	35.4		

Table 5

XPS data of carbon (C–Si, C–C, C–O), silicon (Si–C, SiC_yO_x) and oxygen displayed as at-% versus sputter time for sample P1500.

Time/s	C 1 s/at-%			Si 2p/at-%			O 1 s/at-% overall
	overall	Si-C [at-%]	C-C [at-%]	overall	Si-C [at-%]	SiO _x [at-%]	
0	40	6	94	26	12	88	34
30	27	36	64	37	30	70	36
60	26	50	50	40	37	63	34
120	27	63	37	42	45	55	31
240	29	71	29	44	53	47	27
480	32	80	20	45	63	37	23

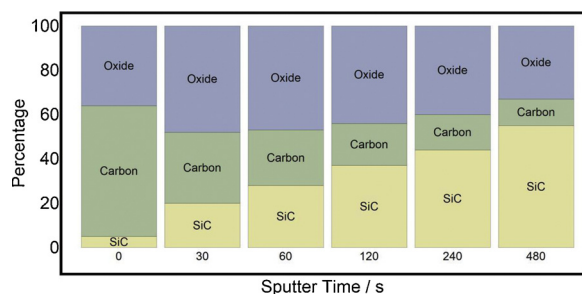


Fig. 8. Surface composition calculated from sputter data (Table 5).

partly oxidized and dissolved into the electrolyte. Again, for sample “P1500” which is characterized by the SiO_x-rich near-surface layer, the C–C/C–Si-peak ratio is strongly increased. This can be explained by the shielding of the inner Si-C phase by the anodic formed SiO₂-film and the selective transformation of Si–C into SiO_x, which leads to a depletion of Si-C in the surface near region. The increase of the C–C/C–Si-peak ratio indicates that the 4-electron reaction (Eq. 1) takes place. Finally, as the sample is measured ex-situ an atmospheric contamination layer contributes to the spectrum. The interpretation of the XPS results can be linked to those of the electrochemical experiments. Sample “P55” which is potentiostatically polarized at E = 55 mV_{SCE} leads solely to a partial removal of carbon. This potential is slightly anodic from the corrosion potential but more negative than the oxidation peak of SiC. This means that a grow of the native passive film by anodic oxidation of SiC should not occur for samples “P55” and “P750” (see Fig. 2). Nevertheless, chemisorption of oxygen prior to the anodic oxidation of the surface can be assumed. However, for sample “P1500” a passivation based on the oxidation (anodization) of the near-surface

region and the formation of a SiO_x surface layer occurs.

The analysis of the depth profile is based on an initial gentle removal of adventitious carbon as described in the experimental part. The resulting evaluation of the sputter profiles of the surface near region are shown in Table 5 and Fig. 8. Fig. 8 graphically illustrates the data in Table 5. The data show that Si(IV)O_x is enriched in the surface near region for sample “P1500”. However, a sharp interface between the SiO_x passive film and the underlying SiC could not be detected. Sputter induced atomic diffusion, a preferential sputtering process and the roughness of the sample surface could all lead to this result. Moreover, it might well be that the surface is chemically not perfectly homogeneous.

4. Conclusion

The corrosion relevant electrochemical behavior of the technical ceramic material EKasic® D in sulfuric acid are investigated. The authors have shown, that these solid-state sintered SiC-ceramics exhibit a very thin native passive film on the samples as received as well as instantaneously formed after the pretreatment in diluted hydro fluorid acid. This film can be described as non-stoichiometric SiOC with a thickness of less than 1 nm. This thin film does not grow in a potential range between the open circuit potential and 1500mV_{SCE}. An oxidation peak observed at approximately E = 230 mV_{SCE} can be explained by oxidation of a very thin surface carbon adsorbate layer. At polarization potential close to the electrochemical window of the electrolyte (herein at E = 1500mV_{SCE}) an anodically formed oxide similar to SiO_x was observed by XPS. As shown by complementary XPS and electrochemical analysis, the passive layer formed at a potential of 1500 mV_{SCE} can be described as a SiO_x/SiO_xC_y nanoporous near-surface region. Complementary estimated oxide film thicknesses results to 4–5 nm with a significant amount of embedded water in the vitreous network. This explains the relatively high permittivity of the passive layer in comparison to a hypothetical defect-free SiO_x barrier film. Based on the XPS-data and complementary coulometric calculated oxide thickness, the mechanism of the oxide formation at 1500 mV_{SCE} can only be explained by a 4-electron reaction according to eq. 1 associated with an anodic oxygen evolution of an assumed 20 %–30 % efficiency. The authors assume that oxygen evolution occurs most probably due to resonance tunneling of electrons across the defect-rich passive film.

Declaration of Competing Interest

The authors declare that they have no known competing financial interests or personal relationships that could have appeared to

influence the work reported in this paper

CRedit authorship contribution statement

M. Schneider: Conceptualization, Writing - original draft, Data curation, Visualization. **K. Kremmer:** Investigation, Data curation, Formal analysis. **M. Voigt:** Investigation, Formal analysis, Data curation, Visualization, Writing - original draft. **G. Grundmeier:** Writing - review & editing.

References

- [1] J.B. Cassidy, R.W. Johnson, Status of silicon carbide (SiC) as a wide-bandgap semiconductor for high-temperature applications: a review, *Solid. Electron.* 39 (1996) 1409–1422.
- [2] L.M. Porter, R.F. Davis, A critical review of ohmic and rectifying contacts for silicon carbide, *Mat. Sci. Eng. B34* (1995) 83–105.
- [3] P.M. Sarro, Silicon carbide as a new MEMS technology, *Sens. Actuators* 82 (2000) 210–218.
- [4] R. Memming, Photochemical and electrochemical processes of excited dyes at semiconductor and Metal electrodes, *Photochem. Photobiol.* 16 (1972) 325–333.
- [5] M. Gleria, R. Memming, Charge transfer process at large band gap semiconductor electrodes: reactions at SiC-electrodes, *J. Electroanal. Chem.* 65 (1975) 163–175.
- [6] J.O.M. Bockris, K. Uosaki, The rate of the photoelectrochemical generation of hydrogen at p-type semiconductor, *J. Electrochem. Soc.* 124 (1977) 1348–1355.
- [7] I. Lauermann, R. Memming, D. Meissner, Electrochemical properties of Silicon Carbide, *J. Electrochem. Soc.* 144 (1997) 73–80.
- [8] C. Schnabel, M. Wörner, B. Gonzalez, I. del Olmo, A.M. Braun, Photoelectrochemical characterization of p- and n-doped single crystalline silicon carbide and photoinduced reductive dehalogenation of organic pollutants at p-doped silicon carbide, *Electrochim. Acta* 47 (2001) 719–727.
- [9] N.R. Mathews, E.L. Miller, P.J. Sebastian, M.M. Hernandez, X. Mathews, S.A. Gamboa, Electrochemical characterization of α -SiC in different electrolytes, *Int. J. Hydrogen Energy* 29 (2004) 941–944.
- [10] P. Simon, A. Burke, *Nanostructured Carbons: Double-Layer Capacitance and More*, Interface Spring, 2008, pp. 38–43.
- [11] R. Wu, K. Zhou, C.Y. Yue, J. Wie, Y. Pan, Recent progress in synthesis, properties and potential applications of SiC nanomaterials, *Progr. Mat. Sci.* 72 (2015) 1–60.
- [12] J.P. Alper, M.S. Kim, M. Vincent, B. Hsia, V. Radmilovic, C. Carraro, R. Maboudian, Silicon carbide nanowires as highly robust electrodes for microsupercapacitors, *J. Power Sources* 230 (2013) 298–302.
- [13] D. Tang, R. Yi, W. Zhang, Z. Qiao, Y. Liu, Q. Huo, D. Wang, Bottom-up synthesis of mesoporous carbon/silicon carbide composite at low temperature for supercapacitor electrodes, *Mat. Lett.* 198 (2017) 140–143.
- [14] L. Gu, Y. Wang, Y. Fang, R. Lu, J. Sha, Performance characteristics of supercapacitor electrodes made of silicon carbide nanowires grown on carbon fabric, *J. Power Sources* 243 (2013) 648–653.
- [15] C. Schmalzried, K.H. Schwetz, Silicon carbide and boron carbide based hard materials, in: R.C. Chen (Ed.), *Ceramic Science and Technology*, Wiley VCH, 2010, pp. 131–225.
- [16] N.D. Shcherban, Review on synthesis, structure, physical and chemical properties and functional characteristics of porous silicon carbide, *J. Ind. Eng. Chem.* (2017), <https://doi.org/10.1016/j.jiec.2017.02.002>.
- [17] K.A. Schwetz, J. Hassler, Zur Beständigkeit von Hochleistungskeramiken gegen Flüssigkorrosion, *cfi/Ber DKG* 79 (2002) D15–8.
- [18] K.A. Schwetz, J. Hassler, Zur Beständigkeit von Hochleistungskeramiken gegen Flüssigkorrosion, *cfi/Ber DKG* 79 (11) (2002) D14–9.
- [19] M. Herrmann, J. Schilm, G. Michael, Corrosion behaviour of different technical ceramics in acids, basic solutions and under hydrothermal condition, *cfi/Ber DKG* 80 (2003) E27–34.
- [20] M. Herrmann, K. Sempf, M. Schneider, U. Sydow, K. Kremmer, A. Michaelis, Electrochemical corrosion of silicon carbide ceramics in H₂SO₄, *J. Eur. Ceram. Soc.* 34 (2014) 229–235.
- [21] F. Meschke, A. Kailer, Electrically driven cold water corrosion of SiC, *cfi/Ber DKG* 81 (2004) E19–22.
- [22] R. Divakar, S.G. Seshadri, M. Srinivasan, Electrochemical techniques for corrosion rate determination in ceramics, *J. Am. Ceram. Soc.* 72 (1989) 780–784.
- [23] S.G. Cook, J.A. Little, J.E. King, Corrosion of silicon carbide ceramics using conventional and electrochemical methods, *Br. Corros. J.* 29 (1994) 183–185.
- [24] A. Andrews, M. Herrmann, M. Sephton, Electrochemical corrosion testing of slid state sinterd silicon arbide in acidic and alkaline environments, *J. South Afr. Inst. Min. Metal.* 106 (2006) 269–276.
- [25] U. Sydow, K. Sempf, M. Herrmann, M. Schneider, H.-J. Kleebe, A. Michaelis, Electrochemical corrosion of liquid phase sintered silicon carbide ceramics, *Mat. Corr.* 64 (2013) 218–224.
- [26] M.S. Antelmann, *The Encyclopedia of Chemical Electrode Potentials*, Plenum, New York, 1982, pp. 101–103.
- [27] A.J. Bard, R. Parsons, J. Jordan, A.J. Bard (Ed.), *Electroanalytical Chemistry and Electrochemistry*, Marcel Dekker, New York, 1985, pp. 189–206 566-580, 587-629.
- [28] J.E. Spanier, A.C. West, I.P. Herman, Electrochemical impedance spectroscopy of 6H-SiC in aqueous hydrofluoric acid, *J. Electrochem. Soc.* 148 (2001) C663–C667.
- [29] A. Andrews, M. Herrmann, M. Sephton, Chr. Machio, A. Michaelis, Electrochemical corrosion of solid and liquid phase sintered silicon carbide in acidic and alkaline environments, *J. Eur. Ceram. Soc.* 27 (2007) 2127–2135.
- [30] V.A. Lavrenko, E.I. Vishnyakova, V.A. Shvets, Electrochemical Properties of sintered polycrystalline α -SiC, *Powder Metall. Met. Ceram.* 43 (2004) 489–496.
- [31] V. Presser, O. Krummhauser, A. Kailer, K.G. Nickel, In situ monitoring and depth-resolved characterization of wet wear of silicon carbide, *Wear* 271 (2011) 2665–2672.
- [32] H. Knoch, M. Fundus, Sintered silicon carbide for slide bearings and seal rings, *Seal. Technol.* 17 (1995) 6–14.
- [33] G. Wötting, W. Martin, Dense SiC-ceramics with specifically adjusted electrical resistance (or electrical conductivity), *Ceramic Appl.* 2 (2014) 50–53.
- [34] <http://www.chemie.de/lexikon/Siliciumdioxid.html> 07.02.2017.
- [35] A.H. Carim, M.M. Dovek, C.F. Quate, R. Sinclair, C. Vorst, High-resolution Electron microscopy and scanning tunneling microscopy of native oxides on silicon, *Science* 237 (1987) 630–632.
- [36] J.O.M. Bockris, S.U.M. Khan, *Surface Electrochemistry—A Molecular Level Approach*, Plenum Press, New York, 1993, <https://doi.org/10.1007/978-1-4615-3040-4>.
- [37] R. Gleria, R. Memming, Charge transfer processes at large band gap semiconductor electrodes: reactions at SiC-electrodes, *J. Electroanal. Chem.* 65 (1975) 163–175.
- [38] D.R. Lide, *Handbook of Chemistry and Physics CRC Press Boca Raton FL*, 73rd ed., (1992), pp. 12–46 -1993.
- [39] M. Fayollea, J. Torres, G. Passemard, F. Fusalba, G. Fanget, D. Louis, M. Assous, O. Louveau, M. Rivoire, K. Haxaire, M. Mourier, S. Maitrejean, P. Besson, L. Broussous, L. Arnaud, H. Feldis, Integration of Cu/SiOC in Cu dual damascene interconnect for 0.1- μ m technology, *Microelectron. Eng.* 64 (2002) 35–42.
- [40] Bing Yang, W.E. Kaden, X. Yu, J.A. Boscoboinik, Y. Martynova, L. Lichtenstein, M. Heyde, M. Sterrer, R. Wlodarczyk, M. Sierka, J. Sauer, S. Shaikhutdinov, H.-J. Freund, Thin silica films on Ru(0001): monolayer, bilayer and three-dimensional networks of [SiO₄] tetrahedral, *Phys. Chem. Chem. Phys.* 14 (2012) 11344–11351.
- [41] M. Morita, T. Ohmi, E. Hasegawa, M. Kawakami, M. Ohwada, Growth of native oxide on silicon surface, *J. Appl. Phys.* 68 (1990) 1272–1281.
- [42] T. Takahagi, I. Nagai, A. Ishitani, H. Kuroda, Y. Nagasawa, The formation of hydrogen passivated silicon single-crystal surfaces using ultraviolet cleaning and HF etching, *J. Appl. Phys.* 64 (1988) 3516–3521.
- [43] A.F. Hollemann, E. Wiberg, *Lehrbuch der Anorganischen Chemie*, Walter de Gruyter Berlin, New York, 1985, pp. 757–764.
- [44] G. Zhang, *Electrochemistry of silicon and ist oxide*, Springer Science + Business Media, LLC N.Y., 2001, pp. 119–120.
- [45] J.W. Schultze, M.M. Lohrengel, Stability, reactivity and breakdown of passive films. Problems of recent and future research, *Electrochim. Acta* 45 (2000) 2499–2513.
- [46] J.W. Schultze, P. Kohl, M. Lohrengel, U. Stimming, Einfluß Von Oxidschichten Auf Elektrodenprozesse, *Chem.-Ing.-Tech* 51 (1979) 643–649 (in German).
- [47] J.A.L. Dobbelaar, E.C.M. Herman, J.H.W. de Wit, The influence of the microstructure on the corrosion behaviour of Fe-25Cr, *Corr. Sci.* 33 (1992) 779–790.
- [48] H. Hasegawa, S. Arimoto, H. Yamamoto, H. Ohno, Anodic oxidation of hydrogenated amorphous silicon and properties of oxide, *J. Electrochem. Soc.* 135 (1988) 424–431.
- [49] J.H. Anderson, G.A. Parks, The electrical conductivity of silica gel in the presence of adsorbed water, *J. Phys. Chem.* 72 (1968) 3662–3668.
- [50] R. Alfonsetti, L. Lozzi, M. Passacandanto, P. Picozzi, S. Santucci, XPS studies on SiOx thin films, *Appl. Surf. Sci.* 70 (1993) 222.
- [51] T.A. Carlson, *Basic Assumptions and Recent Developments in Quantitative XPS*, Surf. Interface Anal. 4 (1982) 125.
- [52] B.R. Strohmeier, An ESCA method for determining the oxide thickness on aluminum alloys, *Surf. Interface Anal.* 15 (1990) 51–56.
- [53] Y. Mizokawa, K.M. Geib, C.W. Wilmsen, Characterization of (3-SiC) surfaces and the Au/SiC interface, *J. Vac. Sci. Technol. A* 4 (1986) 1696.
- [54] R.C. Lee, C.R. Aita, N.C. Tran, The air-exposed surface of sputter deposited silicon carbide studied by x-ray photoelectron spectroscopy, *J. Vac. Sci. Technol. A* 9 (1991) 1351.
- [55] NIST X-ray Photoelectron Spectroscopy Database Version 4.1, NIST Standard Reference Database Number 20, National Institute of Standards and Technology, Gaithersburg MD, 2000 20899.